Springer Tracts in Mechanical Engineering

Esteban Ferrer
Adeline Montlaur *Editors*

CFD for Wind and Tidal Offshore Turbines

Springer

Esteban Ferrer • Adeline Montlaur
Editors

CFD for Wind and Tidal Offshore Turbines

Springer

Editors
Esteban Ferrer
School of Aeronautics
Universidad Politecnica de Madrid
(ETSIA-UPM)
Madrid
Spain

Adeline Montlaur
Universitat Politecnica de Catalunya
Escola d'Enginyeria de Telecomunicacio i
Aeronautica
Catelldefels
Spain

ISSN 2195-9862 ISSN 2195-9870 (electronic)
Springer Tracts in Mechanical Engineering
ISBN 978-3-319-16201-0 ISBN 978-3-319-16202-7 (eBook)
DOI 10.1007/978-3-319-16202-7

Library of Congress Control Number: 2015942220

Springer Cham Heidelberg New York Dordrecht London
© Springer International Publishing Switzerland 2015
This work is subject to copyright. All rights are reserved by the Publisher, whether the whole or part of the material is concerned, specifically the rights of translation, reprinting, reuse of illustrations, recitation, broadcasting, reproduction on microfilms or in any other physical way, and transmission or information storage and retrieval, electronic adaptation, computer software, or by similar or dissimilar methodology now known or hereafter developed.
The use of general descriptive names, registered names, trademarks, service marks, etc. in this publication does not imply, even in the absence of a specific statement, that such names are exempt from the relevant protective laws and regulations and therefore free for general use.
The publisher, the authors and the editors are safe to assume that the advice and information in this book are believed to be true and accurate at the date of publication. Neither the publisher nor the authors or the editors give a warranty, express or implied, with respect to the material contained herein or for any errors or omissions that may have been made.

Printed on acid-free paper

Springer International Publishing AG Switzerland is part of Springer Science+Business Media (www.springer.com)

Springer Tracts in Mechanical Engineering

Board of editors

Seung-Bok Choi, Inha University, Incheon, South Korea
Haibin Duan, Beijing University of Aeronautics and Astronautics, Beijing, P.R. China
Yili Fu, Harbin Institute of Technology, Harbin, P.R. China
Jian-Qiao Sun, University of California, Merced, U.S.A

About this Series

Springer Tracts in Mechanical Engineering (STME) publishes the latest developments in Mechanical Engineering - quickly, informally and with high quality. The intent is to cover all the main branches of mechanical engineering, both theoretical and applied, including:

- Engineering Design
- Machinery and Machine Elements
- Mechanical structures and stress analysis
- Automotive Engineering
- Engine Technology
- Aerospace Technology and Astronautics
- Nanotechnology and Microengineering
- Control, Robotics, Mechatronics
- MEMS
- Theoretical and Applied Mechanics
- Dynamical Systems, Control
- Fluids mechanics
- Engineering Thermodynamics, Heat and Mass Transfer
- Manufacturing
- Precision engineering, Instrumentation, Measurement
- Materials Engineering
- Tribology and surface technology

Within the scopes of the series are monographs, professional books or graduate textbooks, edited volumes as well as outstanding PhD theses and books purposely devoted to support education in mechanical engineering at graduate and post-graduate levels.

More information about this series at
http://www.springer.com/series/11693

此为试读,需要完整PDF请访问: www.ertongbook.com

Introduction

The International Energy Agency (IEA) concludes in The World Energy Outlook 2008 that the current energy consumption and production is "patently unsustainable environmentally, economically, and socially". Social concern and international agreements (e.g. Kyoto 1997, Copenhagen 2009 or Durban 2011) are pushing forward the development of renewable energy technologies for sustainable and renewable energy generation.

In particular, offshore wind and tidal turbines have seen increasing interest from academia, industry and government bodies, during recent years, as offshore sites present huge energy potential. The new engineering challenges presented by these technologies, together with the difficulty to undertake experimental test under offshore environments, have raised the interest on Computational Fluid Dynamics (CFD) to design appropriate turbines and blades, understand fluid flow physical phenomena associated with offshore environments and predict power production, among others.

This book encompasses novel CFD techniques to compute offshore wind and tidal applications. All the included papers have been presented at the 11th World Congress on Computational Mechanics (WCCM XI) organised together with the 6th European Conference on Computational Fluid Dynamics (ECFD VI) in Barcelona 2014. The book includes contributions of researchers from academia and industry.

December 2014
Barcelona, Spain

Esteban Ferrer
Adeline de Montlaur

Contents

Chapter 1
Flow Scales in Cross-Flow Turbines

Esteban Ferrer and Soledad Le Clainche

Abstract This work presents analytical estimates for various flow scales encountered in cross-flow turbines (i.e. Darrieus type or vertical axis) for renewable energy generation (both wind and tidal). These estimates enable the exploration of spatial or temporal interactions between flow phenomena and provide quantitative and qualitative bounds of the three main flow phenomena: the foil scale, the vortex scale and wake scale. Finally using the scale analysis, we show using an illustrative example how high order computational methods prove beneficial when solving the flow physics involved in cross-flow turbines.

1.1 Introduction

Problems where the forces on rotating or oscillating bodies in a fluid are to be predicted are common in engineering applications and result in fluid–structure interaction situations. Examples are flows around isolated rotating bodies and foils, turbomachinery applications, insect flight aerodynamics, unmanned air vehicles and, more recently, flows through renewable energy devices, e.g. wind and tidal turbines.

A particularly challenging problem is presented by cross-flow wind and tidal turbines for power generation (also known as vertical-axis, H-rotors or Darrieus turbines). These types of turbine consist of foil shaped blades that generate lift forces so as to rotate a shaft to which the blades are connected. Therefore azimuthal changes in blade aerodynamics (or hydrodynamics)[1] are common, resulting in

[1]Airfoil aerodynamics and hydrofoil hydrodynamics are equivalent nomenclatures for foils operating in air or water environments. Since this work encompasses both wind and tidal turbine applications, from this point onwards, "foils" will denote either "airfoils" or "hydrofoils". In addition, the term "aerodynamic" can always be replaced by "hydrodynamic" in this work.

E. Ferrer (✉) • S. Le Clainche
ETSIA-UPM - School of Aeronautics, Plaza Cardenal Cisneros 3, 28040 Madrid, Spain
e-mail: esteban.ferrer@upm.es; soledad.leclainche@upm.es

© Springer International Publishing Switzerland 2015

E. Ferrer, A. Montlaur (eds.), *CFD for Wind and Tidal Offshore Turbines*,
Springer Tracts in Mechanical Engineering, DOI 10.1007/978-3-319-16202-7_1

complex flow phenomena such as stalled flows, vortex shedding and blade–vortex interactions.

Cross-Flow Turbines (CFT) are sometimes referred to as vertical-axis turbines, however the term cross-flow turbine is preferred since the absolute turbine position is omitted and the relative flow-axis geometry is emphasised through this terminology.

To date, this type of turbine configuration has had limited use within the wind energy sector, where the three bladed axial flow turbine has been widely adopted. However, it is thought that CFT configurations can be advantageous for new emergent markets as offshore wind and tidal energy production and also for installation in urban environments. A brief review of some of the arguments in favour and against this type of configuration follows. A more complete discussion can be found in [6].

On the one hand, the main drawback is that CFT are generally less efficient than axial flow turbines since the downstream half of the turbine produces less torque due to the shadowing from the upstream blades. Furthermore, since for part of the cycle the blade moves parallel to the flow, the lift force powering the blades, being proportional to the incident flow speed squared, is reduced.

On the other hand, this type of device has the advantage of not requiring a specific orientation relative to the flow, since it can work independently of the stream direction and hence some researchers argue that this technology is more suitable for the offshore environment (offshore wind and tidal) as it would minimise maintenance costs through reduced control systems (e.g. yaw mechanism) [11, 12]. Furthermore, due to its geometrical simplicity, the generator can be located far from the rotating blades, reducing installation complexity and maintenance cost.

To the authors' knowledge, the analysis presented herein is a first attempt to derive analytical estimates that may be used in the future in simplified models of blade element momentum type. The analytical bounds included in this study may provide limiting conditions for analytical models (e.g. [16, 20, 21, 25] for cross-flow wind turbines or [5, 13, 24] in the tidal energy context).

This chapter characterises various physical phenomena encountered in cross-flow turbines and quantifies its spatial and temporal importance in terms of length, time and velocity scales. The quantification of the various physical phenomena provides guidelines for the appropriate simulation of CFT using numerical techniques (e.g. spatial and temporal resolution). Finally, in Sect. 1.4, we address the necessity of high accuracy when computing cross-flow turbine flows using numerical techniques, such as the high order Discontinuous Galerkin method developed by the first author [7–10].

1.2 Physical Characterisation of Cross-Flow Turbine Flows

Both wind and tidal CFT technologies operate at relatively low flow speed, when compared to the speed of sound in their respective media, minimising the effects of fluid compressibility. Typical CFT flows can be characterised using the incompressible Navier–Stokes equations. This system of non-linear partial differential equations can be written in its convective form as the set:

$$\text{Continuity}: \quad \nabla \cdot \mathbf{u} = 0, \tag{1.1}$$

$$\text{Momentum}: \quad \frac{\partial \mathbf{u}}{\partial t} + (\mathbf{u} \cdot \nabla)\mathbf{u} = -\frac{1}{\varrho}\nabla p + \nu \nabla^2 \mathbf{u}, \tag{1.2}$$

where $\mathbf{u} = (u, v, w)^T$ is the vector of the velocity components in three dimensions, p represents the static pressure, ϱ is the density and $\nu = \frac{\mu}{\varrho}$ is the kinematic viscosity, with μ the dynamic viscosity.

The previously defined Navier–Stokes equations can be written in non-dimensional form using the following non-dimensional variables:

$$\mathbf{u}^* = \frac{\mathbf{u}}{U}, \quad p^* = \frac{p}{\varrho U^2}, \quad t^* = t\frac{U}{L}, \quad \nabla^* = L\nabla, \tag{1.3}$$

where, in addition to the defined variables, the following scalars are introduced: U as the characteristic flow velocity (e.g. the freestream speed) and L as the characteristic flow length. Substitution of the non-dimensional quantities into Eq. (1.2) leads to a non-dimensional momentum equation:

$$\frac{\partial \mathbf{u}^*}{\partial t^*} + (\mathbf{u}^* \cdot \nabla^*)\mathbf{u}^* = -\nabla^* p^* + \frac{1}{\mathrm{Re}}\nabla^{*2}\mathbf{u}^*, \tag{1.4}$$

where $\mathrm{Re} = LU/\nu$ is the Reynolds number.

Let us estimate the Reynolds numbers to characterise the flows for wind and tidal turbines. Table 1.1 shows characteristic fluid properties for air (at 15 °C) and sea water (at 0 °C and moderate salinity). The table also includes typical mean flow speeds at wind [3] and tidal sites [5, 18]. As can be seen, both fluids are similar in

Table 1.1 Air and sea water fluid and flow properties

	Units	Air	Sea water
Fluid property			
Density (ϱ)	kg/m^3	~1.225	~1,027
Dynamic viscosity (μ)	Pa s	$\sim 1.78 \times 10^{-5}$	$\sim 1.88 \times 10^{-3}$
Kinematic viscosity (ν)	m^2/s	$\sim 1.45 \times 10^{-5}$	$\sim 1.83 \times 10^{-6}$
Flow property			
Mean flow speed	m/s	~12	~1.5

此为试读,需要完整PDF请访问: www.ertongbook.com

terms of their kinematics: $U_{\text{air}}/\nu_{\text{air}} \sim U_{\text{sea}}/\nu_{\text{sea}}$. To estimate the Reynolds numbers, let us consider a small cross-flow turbine of radius $R = 5\,\text{m}$ (e.g. a wind turbine for urban environment and a typical tidal turbine), then the Reynolds number Re_D based on the turbine diameter D results in $\text{Re}_D{}^{\text{air}} \approx \text{Re}_D{}^{\text{water}} \approx 4 \times 10^6$, showing that from a flow dynamic point of view both technologies operate in similar regimes.

Remark When tidal turbine flows are considered, the Froude number $\text{Fr} = U/\sqrt{gL}$ may be of importance. However for mildly blocked configurations (i.e. low ratio of turbine diameter to shallow water depth) this parameter can be shown to have a relatively low importance [5, 15] and will not be considered in this chapter.

1.3 Disparity of Flow Scales and Their Simulation

This section describes the range of flow scales expected when simulating cross-flow turbine flows in relation to the resolution accuracy required for its simulation. Figure 1.1 presents a schematic illustration of the three physical spatial scales expected on CFT flows: the foil scale, the vortex scale and wake scale. The foil scaling includes near wall scales and boundary layers, the vortex scaling considers vortex shedding and blade–vortex interaction effects and finally the wake scaling includes shadowing effects due to the turbine blockage [5, 15, 23] and the wake structure related to the rotating blades. In this section, estimates for the length, time and velocity scales for the different phenomena are introduced.

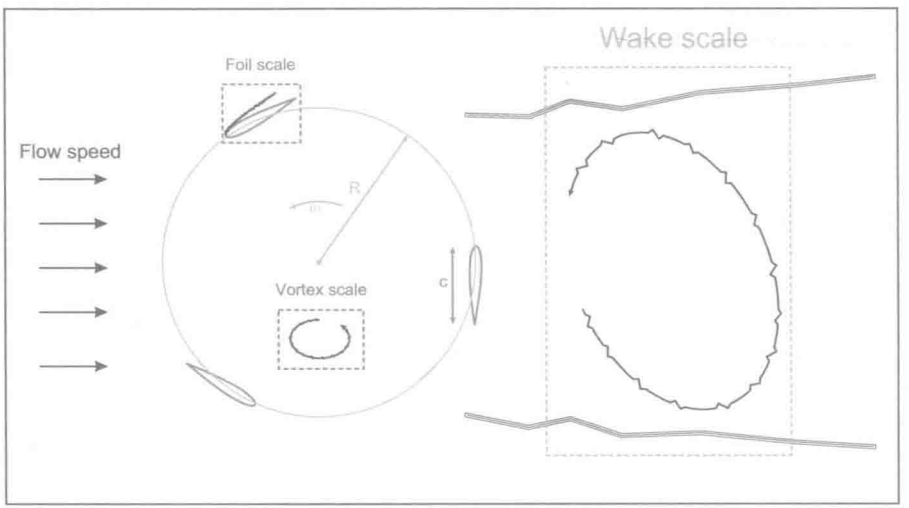

Fig. 1.1 Flow scales in cross-flow turbine flows. Turbine blades of chord c rotate with an angular velocity ω at a distance R from the turbine centre

1.3.1 The Foil Scaling

In the presence of a non-slip condition at the wall surface, the flow is forced to slow down to have zero velocity at the wall. This creates the so-called boundary layer (defined by Prandtl in 1904) that will develop on turbine blades. The logarithmic profile of tangential velocities developed at the wall (if attached flow is considered) has to be properly modelled in a numerical simulation, since it directly influences the aerodynamic forces on the blades. Typically, the foil boundary layer has a laminar portion which will undergo transition to turbulence some distance downstream (assuming a high enough Reynolds number); this distance being influenced by, among other factors, the pressure gradient on the surface, the wall surface roughness and the free stream turbulence outside the boundary layer. Turbulent boundary layers are thicker and carry more momentum and thus separate later than laminar boundary layers. Boundary layers are a vast topic of research and only the principal characteristics have been outlined here. For a detailed explanation the reader is referred to the monograph by Schlichting [19].

It is possible to estimate CFT's length scales for the boundary layer using the Blasius approximation [19] for the flow over a flat plate with zero pressure gradient. First, let us consider the rotational speed of the blades $U_{\text{rot}} = \omega R$, where ω is the angular velocity and R the turbine radius. In addition, we define the tip speed ratio as $\lambda = U_{\text{rot}}/U$, where U represents the free stream velocity. For simplicity, the velocity that the foil experiences can be estimated as $U_{\text{foil}} = \sqrt{U_{\text{rot}}^2 + U^2} \approx U_{\text{rot}} = \lambda U$, which is a valid assumption for $\lambda >> 1$ (i.e. ignoring the free stream velocity U). Then, Blasius' approximation provides a boundary layer of thickness: $\delta \approx x/(\frac{xU_{\text{foil}}}{\nu})^{\gamma} = x/(\frac{x\lambda U}{\nu})^{\gamma}$, where x is the distance from the leading edge and the exponent γ relates to the boundary layer regime: $\gamma = 1/2$ for a laminar regime and $\gamma = 1/5$ for a turbulent boundary layer. By setting $x = c$ (i.e. the foil chord), it is possible to obtain a characteristic length scale for the foil $\ell_{\text{foil}} = \frac{c}{(\text{Re}_{\text{foil}})^{\gamma}}$, where $\text{Re}_{\text{foil}} = \frac{cU_{\text{foil}}}{\nu}$ is the Reynolds number based on the foil chord. An estimate for the time scale can be readily found: $\tau_{\text{foil}} = \frac{\ell_{\text{foil}}}{U_{\text{foil}}} = \frac{c}{U\lambda(\text{Re}_{\text{foil}})^{\gamma}}$. A summary of these scales is given in Table 1.2.

Table 1.2 Characteristic foil scales in CFT turbines

Length scale ℓ_{foil}	Time scale τ_{foil}	Velocity scale U_{foil}	Reynolds number Re_{foil}
$\frac{c}{(\text{Re}_{\text{foil}})^{\gamma}}$	$\frac{c}{U\lambda(\text{Re}_{\text{foil}})^{\gamma}}$	λU	$\frac{c\lambda U}{\nu}$

1.3.2 The Vortex Scaling and Blade–Vortex Interaction

Vortex shedding and vortex impingement may play an important role in turbine performance. For cross-flow turbines, a vortex created by the upstream half of the turbine may be convected downstream, interacting with the rear half of the turbine. Numerical accuracy can significantly influence this phenomenon since vortices may diffuse and lose their structure, changing the forces seen by the rear passing blade. Typically, low order methods (e.g. Finite Volume) have been used to compute CFT flows (e.g. [4, 14, 17]), however, these show non-negligible diffusive and dispersive errors that may disturb flow structures (e.g. vortices or wakes, see [7] for illustrations). In numerical simulations, high order methods (with low numerical errors, e.g. [7, 9]) codes are preferred to capture accurately vortex evolution and blade–vortex interaction phenomena.

An estimate for the scales corresponding to the vortex convection and the blade–vortex interaction phenomenon is provided. Firstly, let us assume a two dimensional vortex with area $A \approx \frac{\pi}{4}c^2$ (the circular area covered by the two dimensional vortex), where c is the characteristic length (the foil chord and the diameter of the vortex) and with characteristic turn over time $\tau_{\text{vortex}} \approx \frac{2\pi}{\omega_z}$, where ω_z represents the vorticity magnitude. By approximating the vorticity as a function of the foil circulation and thus of the lift generated by the foil (Kutta–Joukowski theorem [2]), it is possible to write $\omega_z \approx \frac{\Gamma}{A}$, with $\Gamma = \frac{L}{\varrho U_{\text{foil}}}$ representing the circulation and L the foil lift force. Since $L = \frac{1}{2}\varrho U_{\text{foil}}^2 c C_L$, with C_L the foil lift coefficient, the characteristic vortex time can be expressed as: $\tau_{\text{vortex}} \approx \frac{\pi^2 c}{\lambda U C_L}$. Finally the characteristic velocity of the vortex can be estimated as $U_{\text{vortex}} = \frac{\ell_{\text{vortex}}}{\tau_{\text{vortex}}} \approx \frac{\lambda U C_L}{\pi^2}$.

To estimate the lengths and times of the blade–vortex (BV) interaction phenomenon, let us assume a vortex of diameter c that convects through the turbine at a velocity $U_{\text{axial}} = \beta U$, where $\beta < 1$ represents the velocity deficit through the turbine[2] and U_{axial} is the mean streamwise velocity component within the turbine. The time for a vortex to convect from the front half to the rear half (i.e. to travel the distance $D = 2R$) can be estimated as $\tau_{BV} = \frac{\ell_{BV}}{U_{\text{axial}}} = \frac{D}{\beta U}$. Table 1.3 summarises these scales.

Table 1.3 Characteristic vortex scales in CFT turbines

Length scale ℓ_{vortex}	Time scale τ_{vortex}	Velocity scale U_{vortex}	Reynolds number $\text{Re}_{\text{vortex}}$
c	$\frac{\pi^2 c}{(\lambda U C_L)}$	$\frac{\lambda U C_L}{\pi^2}$	$\frac{c\lambda U C_L}{\pi^2 \nu}$
ℓ_{BV}	τ_{BV}	U_{BV}	Re_{BV}
D	$\frac{D}{\beta U}$	βU	$\frac{D\beta U}{\nu}$

[2] $\beta < 1$ for unblocked cases but may exceed 1 if blockage leads to accelerated flow through the turbine.

Table 1.4 Characteristic wake scales in CFT turbines

Length scale ℓ_{wake}	Time scale τ_{wake}	Velocity scale U_{wake}	Reynolds number Re_{wake}
D	$\frac{D}{\beta\beta' U}$	$\beta\beta' U$	$\frac{D\beta\beta' U}{\nu}$

1.3.3 The Wake Scaling

Cross-flow turbine wake development and dissipation are of major importance since the performance of downstream turbines may be influenced by the structure and strength of upstream generated structures. Furthermore, the wake development modifies the incoming flow speed and consequently angle of attack of the turbine blades. This may alter the performance and efficiency of the turbine and thus its correct prediction is important. Unconfined wakes have been studied for a long time in the context of wind turbines. For example, the paper by Vermeer et al. [22] is an extensive review of experimental and numerical results for axial wind turbine wakes. Although various empirical models exist to predict the extension of the wake behind an operating wind turbine, and many numerical codes have been used to describe the wake structure, the study concludes that more experimental data is needed and that the wake characteristics are still not well understood. However, it seems clear that the wake can be subdivided into a near wake where coherent structures develop, and a far wake, where mixing generates an almost uniform velocity deficit.

Let us estimate the length and time scales for the near wake assuming a wake of diameter $D = 2R$, and a velocity in the wake region as $U_{\text{wake}} = \beta\beta' U$, where in addition to the induction factor β introduced in the previous section, $\beta' < 1$ is defined as the velocity deficit due to the rear half blade passage. The characteristic scales are detailed in Table 1.4.

1.3.4 Scale Comparison and Numerical Resolution

It is possible to compare the different length and time scales obtained for the different phenomena (Tables 1.2, 1.3 and 1.4) to estimate the zones that require more spatial and temporal resolution for a numerical simulation. The most stringent length and time scales are clearly the foil scale since both decrease as the Reynolds number Re_{foil} increases. The vortex time scale is the smallest after the foil time scale but of the same order of magnitude as the blade–vortex interaction scale.

When comparing the time scales for the blade–vortex interaction and the near wake resolution, one can see that $\ell_{\text{wake}} \approx \ell_{BV}$ and $\tau_{\text{wake}} \approx \frac{\tau_{BV}}{\beta'}$, which implies that for $\beta' < 1$ the blade–vortex interaction phenomenon requires smaller temporal resolution than the wake resolution.

In addition, one may examine the factors influencing the separation of scales using the ratios of the smallest to largest scales. Let us define the ratio of length scales as $r_\ell = \frac{\ell_{\text{foil}}}{\ell_{\text{wake}}}$. Substitution of the appropriate length scales (from Tables 1.2 and 1.4) lead to $r_\ell = \frac{c}{D(\text{Re}_{\text{foil}})^\gamma}$. This expression can be further simplified by using the definition of the turbine solidity $\sigma/N = 2c/D$, where N is the number of turbine blades. The final expression for the ratio of length scales reads: $r_\ell = \frac{\sigma}{2N(\text{Re}_{\text{foil}})^\gamma}$. Examination of the last expression shows that the separation of these length scales becomes larger (i.e. smaller ratio) if the number of blades (N) and the Reynolds number (Re_{foil}) increase or the solidity (σ) decreases.

Similarly, a ratio for the time scales can be derived leading to $r_\tau = \frac{\tau_{\text{foil}}}{\tau_{\text{wake}}} = \frac{\sigma\beta\beta'}{2N\lambda(\text{Re}_{\text{foil}})^\gamma}$. In this case, the time scale separation becomes larger if the number of blades (N), the Reynolds number (Re_{foil}) and the tip speed ratio (λ) increase, or the solidity (σ) and induction factors ($\beta\beta'$) decrease. It may be noted, from the derived expressions, that the time scale separation is more restrictive than the length scale separation since: $r_\tau = \frac{\beta\beta'}{\lambda} r_\ell$ with $\beta\beta' < 1$ and $\lambda >> 1$.

To conclude this section, a quantitative estimation of the various scales (Tables 1.2, 1.3 and 1.4) is provided in Table 1.5 for a typical CFT using the air and water environmental conditions introduced in Sect. 1.2. Namely, let us consider a cross-flow turbine of radius $R = 5\,\text{m}$ consisting of airfoils of chord $c = 1\,\text{m}$ (i.e. solidity $\sigma/N = 0.2$). To evaluate the length, time and velocity scales, it is necessary to approximate the following parameters: $\gamma = 1/5$ for a turbulent boundary layer, the tip speed ratio $\lambda \approx 3$, the lift coefficient $C_L \approx 1$ (e.g. maximum C_L for a NACA0015 at $\text{Re} = 1 \times 10^6$ [1]) and the induction factors $\beta \approx \beta' \approx 0.5$. In addition, calculations are performed for two flow speeds $U = 12$ and $1.5\,\text{m/s}$ corresponding to air and water environments respectively (i.e. wind and tidal turbines). Note that the two media require different values for the kinematic viscosity: $\nu = 1.45 \times 10^{-5}$ and $1.83 \times 10^{-6}\,\text{m}^2/\text{s}$ for air and salted water, respectively. Inspection of Table 1.5 reveals that smaller time scales are present

Table 1.5 Summary and evaluation of CFT scales for wind and tidal energy

	Length scale ℓ (m)	Time scale τ (s)	Velocity scale U (m/s)	Reynolds number Re
Wind turbine				
Foil	0.053	0.001	36.000	2.5×10^6
Vortex	1.000	0.274	3.648	2.5×10^5
BV	10.000	1.667	6.000	4.1×10^6
Wake	10.000	3.333	3.000	2.1×10^6
Tidal turbine				
Foil	0.053	0.012	4.500	2.5×10^6
Vortex	1.000	2.193	0.456	2.5×10^5
BV	10.000	13.333	0.750	4.1×10^6
Wake	10.000	26.667	0.375	2.0×10^6

when considering wind turbines over tidal turbines. However, it can be noted that the ratios of time scales (i.e. r_τ) are of the same order for both types of turbines.

The results from this simplified analysis confirm the intuitive reasoning on scale separation. However, it appears useful as it outlines the wide range of length and time scales that need to be accurately simulated to capture correctly the complex flow physics involved in cross-flow turbine simulations. In addition, the analysis allows for quantification of the relative importance of the various flow phenomena.

1.4 Engineering Accuracy and High Accuracy

It is often argued that high accuracy is not compulsory for most engineering applications since an error of 5–10 % may be acceptable and high order techniques are not necessary. In this section we show that the propagation of errors can result in unacceptable inaccuracies when evaluating the performance of CFTs. To exemplify why high accuracy may be of interest, the configuration depicted in Fig. 1.2 is considered. The figure depicts an array of two turbines where the second operates in the wake of the first.

Let us assume that the flow field around the first turbine is accurately resolved up to an error of 5 %: $U = U^{\text{exact}}(1 \pm 0.05)$. Assuming also a 5 % error when calculating U_{axial}, the error in the induction factor $\frac{U_{\text{axial}}}{U} = \beta$ (see Sect. 1.3) can be bounded as $\beta \approx \beta^{\text{exact}}(1 \pm 0.07)$. If the induction factor for the rear half $\beta' = \frac{U_{\text{wake}}}{U_{\text{axial}}}$ has the same errors associated than β (which is clearly a conservative estimate), one obtains $\beta' \approx \beta'^{\text{exact}}(1 \pm 0.07)$. The wake velocity can now be estimated following: $U_{\text{wake}} = \beta\beta' U$ and has bounds $U_{\text{wake}} = \beta^{\text{exact}}\beta'^{\text{exact}}U^{\text{exact}}(1 \pm 0.07)(1 \pm 0.07)(1 \pm 0.05) \approx U^{\text{exact}}_{\text{wake}}(1 \pm 0.11)$. This corresponds to a 11 % error in the incoming velocity for the second turbine. The examples show how an initially "engineering acceptable" error of 5 % may result in unacceptable levels after only one row of turbines. If a similar analysis is performed for the second row, it can be shown that the error increases to 15 % for the wake (assuming the same errors in the induction factors).

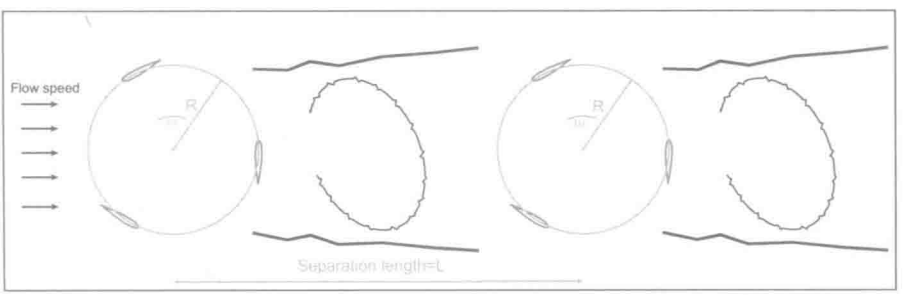

Fig. 1.2 Array of turbines (schematic)

此为试读,需要完整PDF请访问: www.ertongbook.com